JOURNAL OF APPLIED ELECTROCHEMISTRY 25 (1995) 334–339

Calculation of the impedance of noncylindrical pores Part II: Experimental verification on pores drilled into stainless steel

K. ELOOT, F. DEBUYCK, M. MOORS, A. P. VAN PETEGHEM

Laboratorium voor Non-Ferro Metallurgie, Universiteit Gent, Campus Ardoyen, Technologiepark-Zwijnaarde 9, B-9052 Zwijnaarde, Belgium

Received 13 April 1994; revised 21 September 1994

The method of one-dimensional modelling of the pore impedance is validated on pores drilled in AISI 316 stainless steel. Impedance measurements were carried out in 0.5 M sulphuric acid solution. Experimentally, it is found that, for cylindrical pores with a radius/pore length-ratio smaller than 0.5, the one-dimensionality condition is satisfied. Furthermore, impedance measurements on noncylindrical, scaled-up pores provide evidence that a geometric constant Λ_g has to be introduced, as in Part I. In accordance with this theory it is found that for pores with narrowing cross section Λ_g is less than 1/3, while for pores with a broadening cross section Λ_g is greater than 1/3. Moreover, it is shown that the matrix method, presented in Part I, provides a way of calculating the impedance of a noncylindrical pore by using a highly reduced number of discs, N, compared to the recursion method of Keiser *et al.* This is an advantage in fitting procedures.

1. Introduction

In recent literature [1–5] several authors have reported the use of a one-dimensional approach for the modelling of the measured impedance of porous electrodes. The difficulty of such systems is to obtain reliable information about the number, shape, radius and length of the pores. Moreover, the measured impedance of a real porous electrode is composed of the impedances of many pores with different dimensions. These complications make it difficult to confirm experimentally the applicability of the one-dimensional approach for the modelling of pore impedances. Therefore, we have simplified the problem. In this paper we report impedance measurements made on scaled-up pores, obtained by drilling. Pore shape and dimensions were thus well known. The pore impedance was calculated using the matrix method [6].

2. Material and method

Stainless steel AISI 316 was used as electrode material. The resistance of this material can be neglected. This simplifies the calculations as described in Part I [6]. All samples were cleaned and rinsed before starting impedance measurements. Measurements were performed in 0.5 M sulphuric acid solution. The measuring cell was designed so that 1 cm^2 of the working electrode was subjected to the electrolyte. A Luggin capillary was used as electrolyte bridge between the surface of the working electrode and the reference electrode compartment. A Ag/AgCl electrode served as reference. The counter electrode was a platinum perforated plate. A.c. impedance measurements were performed with an EG&G impedance system model 378, which consisted of a potentiostat 273, a lock-in amplifier 5208 and an IBM personal computer. The impedance spectrum was measured in the range 10 mHz to 100 kHz. During measurements the electrolyte was stirred. The amplitude of the a.c.-signal was chosen so that the linearity conditions were satisfied for all frequency ranges.

To characterize the interface reactions between AISI 316 and sulphuric acid, experiments were performed on flat surfaces. Subsequently, the impedance of cylindrical and noncylindrical pores drilled in flat samples was measured.

3. Experimental details

3.1. *Flat surface electrodes*

The impedance Z_{EC} of the equivalent circuit for the measured impedance of a flat AISI 316 electrode immersed in sulphuric acid is given by

$$Z_{EC} = R_e + \frac{Z_w}{A} \quad (1)$$

$R_e(\Omega)$ is the electrolyte resistance and A (cm^2) the surface area of the flat electrode. The specific interface impedance is a parallel combination of a specific resistance R_w ($\Omega\,cm^2$) and a specific impedance of a constant phase element (CPE) Q_w ($\Omega\,cm^2$) = $Q_{0,w}(j\omega)^{-\alpha}$. $Q_{0,w}$ ($\Omega\,cm^2\,s^{-\alpha}$) is a real constant, ω (rad s^{-1}) the circular frequency and in general α lays between 0 and 1. R_w takes into account the charge

0021-891X

transfer and surface resistance due to the passivation reaction and passivation layer at the electrode surface. Q_w is due to the double layer and passivation layer capacity. With the characteristic time constant τ_w

$$\tau_w = \left(\frac{R_w}{Q_{0,w}}\right)^{1/\alpha} \quad (2)$$

Z_w is written

$$Z_w = \frac{R_w}{1 + (j\omega\tau_w)^\alpha} \quad (3)$$

Values of $Q_{0,w}$, R_w, α and R_e were calculated for two flat electrode specimens by nonlinear complex mean square fitting. They are listed in Table 1; the relative error of the parameters is very small. Furthermore, Table 1 shows that $Q_{0,w}$, R_w and α deviate in value for different specimens. However, this lack of reproducibility does not affect the experiments on pores drilled in flat surfaces, because their shape and dimensions are known.

3.2. *Porous electrodes*

For the sake of simplicity measurements were made on pores with insulating pore base and insulating surrounding electrode surface. In this case only the pore wall has contact with the electrolyte. The working electrode plates were made of AISI 316 steel in which pores were drilled. At the bottom of the steel plate a plexiglass plate was attached and the top surface surrounding the pore, was isolated with plexiglue. These pores were subjected to the electrolyte. Special care was taken to prevent enclosing air in the pore. The impedance of the equivalent circuit Z_{EC} of a pore made as described above and immersed in sulphuric acid is given by

$$Z_{EC} = R_e + Z_p \quad (4)$$

The pore impedance Z_p can be calculated by the matrix calculation method as described in Part I. The specific interface impedance to be used in the formulas is given by Equation 3.

In Part I it was pointed out that a pore behaves as an infinitely deep one for the highest frequencies, i.e., lowest penetration depths λ_r. For sufficiently high frequencies, Equation 3 is simplified to

$$Z_w = Q_{0,w}(j\omega)^{-\alpha} \quad \text{for } \omega\tau_w \gg 1 \quad (5)$$

The complex and real penetration depths of the a.c.-signal are, independent of pore shape, given by

$$\lambda_k = \lambda_r\left[1 + j\tan\left(-\alpha\frac{\pi}{4}\right)\right] \quad \text{for } \omega\tau_w \gg 1 \quad (6)$$

Table 1. Experimental values for the different parameters representing the flat electrode surface

	R_e/Ω	$Q_{0,w}/\Omega\,cm^2\,s^{-\alpha}$	α	$R_w/\Omega\,cm^2$
Sample 1	3.9	1.388×10^4	0.89	1.800×10^5
rel. error	1.41%	0.80%	0.23%	5.33%
Sample 2	3.8	2.126×10^4	0.91	1.086×10^5
rel. error	1.37%	0.78%	0.21%	2.87%

$$\lambda_r = \sqrt{\left(\frac{Q_{0,w}r}{2\rho_s\omega^\alpha}\right)}\cos\left(\alpha\frac{\pi}{4}\right) \quad \text{for } \omega\tau_w \gg 1 \quad (7)$$

ρ_s is the specific electrolyte resistance (Ω cm) and r is the mean pore radius (cm). The impedance of an infinitely deep pore is given by

$$Z_{p,\infty} = \left[1 + j\tan\left(-\alpha\frac{\pi}{4}\right)\right]\frac{\lambda_r}{l}R_0 = \frac{\lambda_k}{l}R_0 \quad (8)$$

with

$$R_0 = \frac{\rho_s l}{\pi r^2} \quad (9)$$

and l is the pore depth (cm). $Z_{p,\infty}$ represents the impedance of a CPE having half the phase angle of the CPE given in Equation 5. Furthermore, this impedance is independent of pore shape. When the penetration depth of the a.c.-signal becomes large in comparison with the pore depth, the pore wall behaves as a flat surface [6]. The pore impedance is then given by

$$Z_p = \Lambda_g R_0 + \frac{Z_w}{2\pi r l} \quad (10)$$

with Λ_g the geometry constant (see Part I).

Contrary to normal practice, when measuring on real porous electrodes, r, l and n (number of pores) are known values in these experiments. As a consequence $Q_{0,w}$, α, R_w and ρ_s are to be determined from the measured impedances. This determination was done by two methods. Method 1 involved a nonlinear least square fitting (NLSF) using only the measured impedances at frequencies for which there is 'flat surface behaviour'. Method 2 involved a NLSF-fitting on all measured impedances.

3.2.1. Method 1. From Equation 8 it follows that for the lowest penetration depths the pore behaves as a CPE with phase angle $-\alpha\pi/4$ (Fig. 1). The cross section of the CPE-line with the real axis is equal to R_e. At somewhat lower frequencies both Equations 10 and 5 are valid. This results in a second CPE-line in Fig. 1 having a phase angle of $\alpha\pi/2$. This CPE-line crosses the real axis at R_i. Using all data points at frequencies for which the pore behaves as a flat surface, it is possible to find values for R_i, $Q_{0,w}$, α

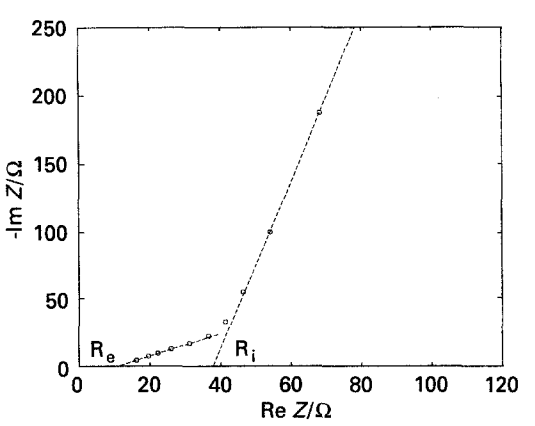

Fig. 1. Definition of R_e and R_i ($\alpha = 0.9$, $\rho_s = 10\,\Omega$cm, $R_e = 10\,\Omega$, $R_w = 10^5\,\Omega\,cm^2$, $Q_{0,w} = 5 \times 10^4\,\Omega\,cm^2\,s^{-\alpha}$, $r = 0.20$ cm, $l = 1$ cm).

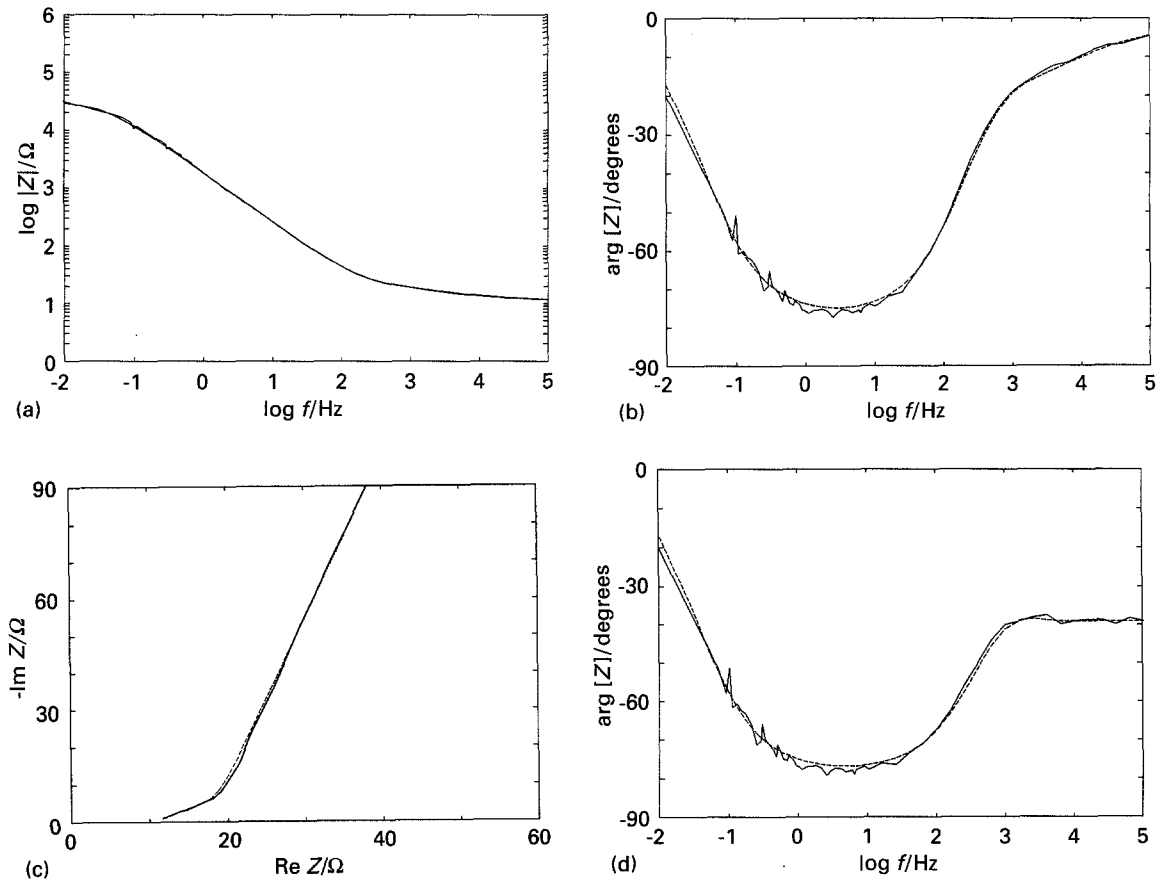

Fig. 2. Measured and simulated pore impedance (pore radius $r = 0.20$ cm, pore length $l = 0.75$ cm). (a) Bode amplitude diagram. (b) Bode phase diagram. (c) Nyquist diagram of the high frequency range. (d) Bode phase diagram for the pure pore impedance (without serial resistance). Key: (——) measured; (· · · · · ·) method 1; (- - - - -) method 2.

and R_w from NLSF-fitting. The electrolyte resistance R_e is found by real linear mean square fitting using the measured data from the CPE-line with phase angle $\alpha\pi/4$ in Fig. 1. Combination of Equations 10, 4 and Fig. 1 leads to

$$\rho_s = \frac{(R_i - R_e)\pi r^2}{\Lambda_g l} \tag{11}$$

3.2.1. Method 2. Using the matrix method [6] and the measured impedances at all frequencies in a NLSF-fit, all the unknown parameters (R_e, $Q_{0,w}$, α, R_w and ρ_s) are found. The main advantage of this method is that it requires only one fitting to obtain the unknown parameters. For method 1 two fittings and the determination of the maximal frequency for flat surface behaviour are necessary. However, a disadvantage of method 2 is that convergence can be a problem when the starting values are not sufficiently good. This is due both to the bigger parameter set and the more complex equation used in method 2. Appropriate starting values for method 2 can be obtained from the NLSF-fitting of method 1. A further advantage of method 1 is that the geometry constant Λ_g appears explicitly in Equation 11. The determination of R_e, R_i, $Q_{0,w}$, α and R_w can be made without knowledge of the pore shape, which is impossible for method 2. Therefore it is useful to evaluate both methods.

4. Results and discussion

4.1. *Experimental verification of the one-dimensionality*

Experimental verification of the assumption of one-dimensionality was performed on cylindrical pores with various combinations of pore radius r and pore length l ($l = 0.25$, 0.5, 0.75 and 1 cm, $r = 0.1$, 0.15, 0.2 and 0.25 cm). Values for the unknown parameter set were obtained from the measured impedances by the two analysing methods. The geometric constant $\Lambda_g = 1/3$ for a cylindrical pore [6]. The verification of one-dimensionality is performed using two criteria. The first is that there should exist a good agreement between the simulated and the measured impedance spectrum especially for the highest frequencies, which are typical for pore behaviour. The second is that the values of ρ_s obtained from all the experiments should be the same since all experiments were done in 0.5 M sulphuric acid.

As an example, the measured impedance spectrum is compared with the simulated one in Fig. 2 for $r = 0.20$ cm and $l = 0.75$ cm. Both Bode diagrams, Fig. 2(a) and (b), are equally sensitive for all frequencies. However, since the pore only 'behaves as a pore' in the highest frequency range, a Nyquist plot of this range provides a more sensitive presentation of the measured and calculated data, Fig. 2(c). Another useful and very sensitive diagram is obtained when the pore impedance Z_p, that is, the

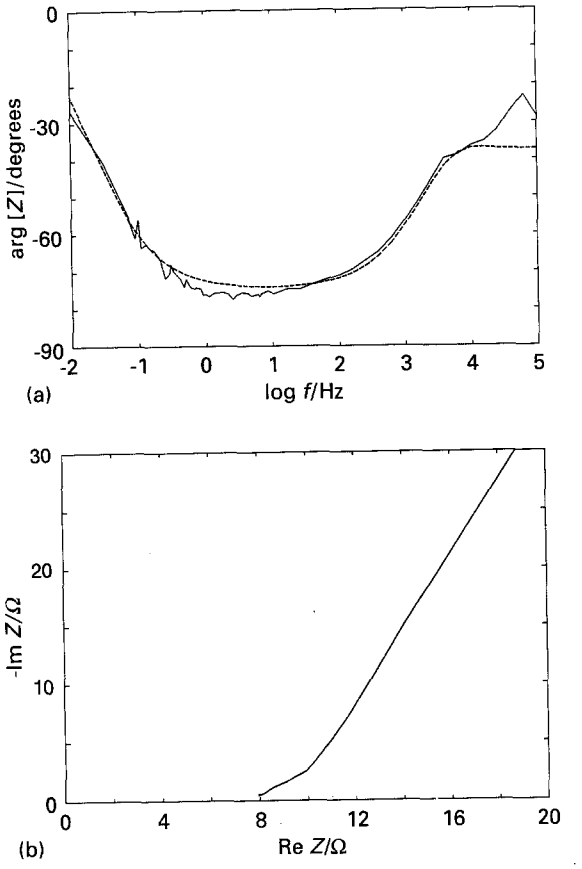

Fig. 3. (a) Bode phase diagram for the pure pore impedance with ratio $r/l = 1$ (pore radius $r = 0.25$ cm, pore length $l = 0.25$ cm). (b) Nyquist diagram of the high frequency range of the measured impedances. Key: (——) measured; (- - - -) method 2.

measured impedance minus the electrolyte resistance ($Z_{EC} - R_e$), is placed in a phase diagram, Fig. 2(d). The perfect agreement seen in Fig. 2 between the two fitting methods, can be generalized to almost all r/l-combinations.

Evaluating the first criterion, it is found that the agreement between the measured and calculated impedances for high frequencies (i.e., higher than 10^3 to 10^4 Hz, depending on the pore dimensions) is worst for $r/l = 1$, Fig. 3. The agreement is somewhat better for $r/l = 0.8$, Fig. 4, and $r/l = 0.6$. A very good agreement is found for $r/l \leqslant 0.5$ (e.g., Fig. 2 for $r/l = 0.27$).

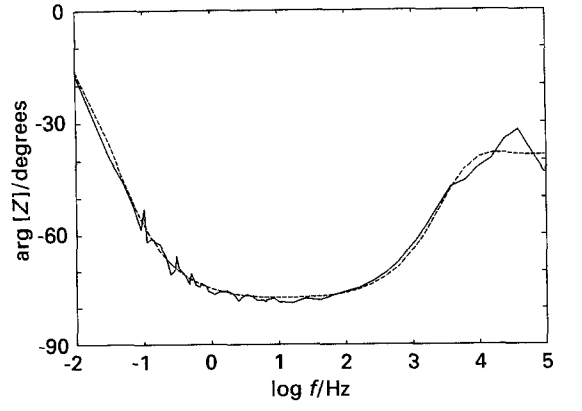

Fig. 4. Bode phase diagram for the pure pore impedance with ratio $r/l = 0.8$ (pore radius $r = 0.20$ cm, pore length $l = 0.25$ cm). Key: (——) measured; (- - - -) method 2.

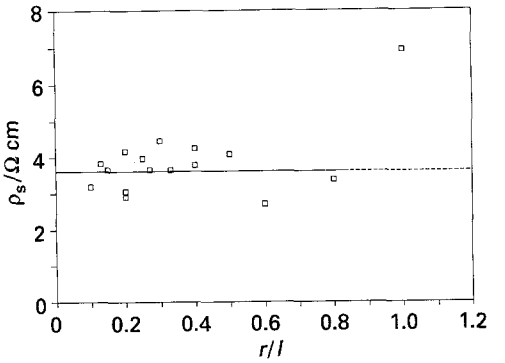

Fig. 5. Specific electrolyte resistance ρ_s as function of the ratio r/l (data from method 2).

The second criterion is evaluated graphically in Fig. 5, from which a roughly constant mean value was found for $r/l \leqslant 0.8$, namely $3.65 \pm 0.5\,\Omega$ cm, which is somewhat lower than that from the literature (4.68 Ω cm at 20° C) [8]. For $r/l = 1$ a resistivity value of 6.92 Ω cm was found. This is a second indication that for $r/l = 1$ the 'pore' cannot be considered as a one-dimensional electrochemical system for the highest frequencies.

From evaluation of the two criteria for a one dimensional approach, it is concluded that for $r/l \leqslant 0.5$ the one dimensional modelling of the pore impedance is possible.

It is worth noting that for $r/l = 1$ the Nyquist plot at the lowest penetration depths shows the typical 'pore behaviour', as can be seen from comparison of Fig. 3(b) and Fig. 1. The reason why a clearly increased resistivity value (6.92 Ω cm) is found for this typical 'pore behaviour curve' can be explained qualitatively. Since the diameter of the pore is large compared to the pore length ($d = 2l$), the current will not spread homogeneously across the complete pore section at the highest frequencies (lowest penetration depths) (Fig. 6). The current always follows the path with lowest resistivity, resulting in a higher concentration at the pore wall compared to the middle of the pore section. Formally, this phenomenon could be called the 'skin-effect'. The apparent curvature of the equipotential surfaces cannot be neglected, making one dimensional modelling impossible. However, supposing that no current flows at the centre of the pore, the current density curve a from

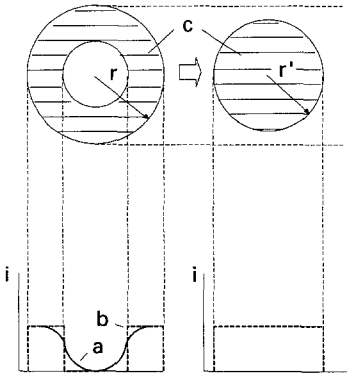

Fig. 6. Schematic view of the current density over the pore section when the one dimensionality condition is lost.

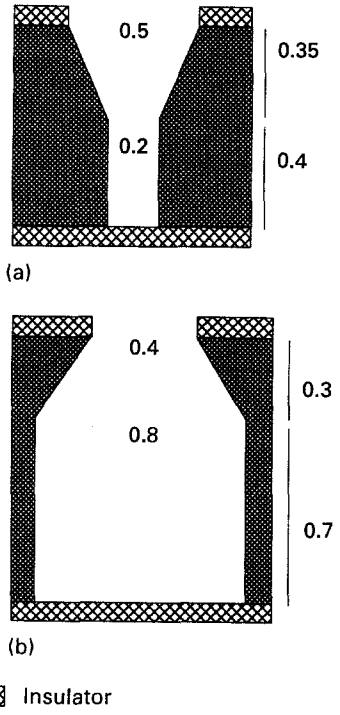

Fig. 7. The noncylindrical pore shapes (length and diameter are mentioned in cm).

Fig. 6 can be changed into b. For this case only part of the pore section is used (the shaded area c). This leads to a smaller virtual pore section c and to a smaller virtual pore radius r', compared to the real section and radius. Using Equation 11 and the mean specific electrolyte resistance $\rho_s = 3.65\,\Omega$, the virtual pore radius (in cm) is given by

$$r' = \frac{r}{1.37} \tag{12}$$

This result proves that at low penetration depths only a part of the pore section is used by the current in the case of $r/l = 1$.

4.2. *Experimental verification of the geometry constant* Λ_g

In Part I it was shown theoretically that, for high penetration depths, the real part of the normalized (i.e., divided by R_0) pore impedance depends on the pore shape. Therefore a geometry constant Λ_g was introduced. Keiser *et al.* [7] claimed that this constant is independent of the shape and equal to 1/3. Although it was already proved theoretically in Part I that this is wrong, it will now be confirmed experimentally. Impedance measurements were performed on scaled-up pores with variable cross section. These

Table 2. The fitted specific electrolyte resistance ρ_s as function of the geometry constant Λ_g

Pore shape	*r*/cm *(mean)*	*l*/cm	Λ_g *(theoretical)*	ρ_s/Ωcm	
				method 1	*method 2*
a	0.135	0.75	0.169	2.27	2.31
b	0.370	1.00	0.550	5.01	5.12

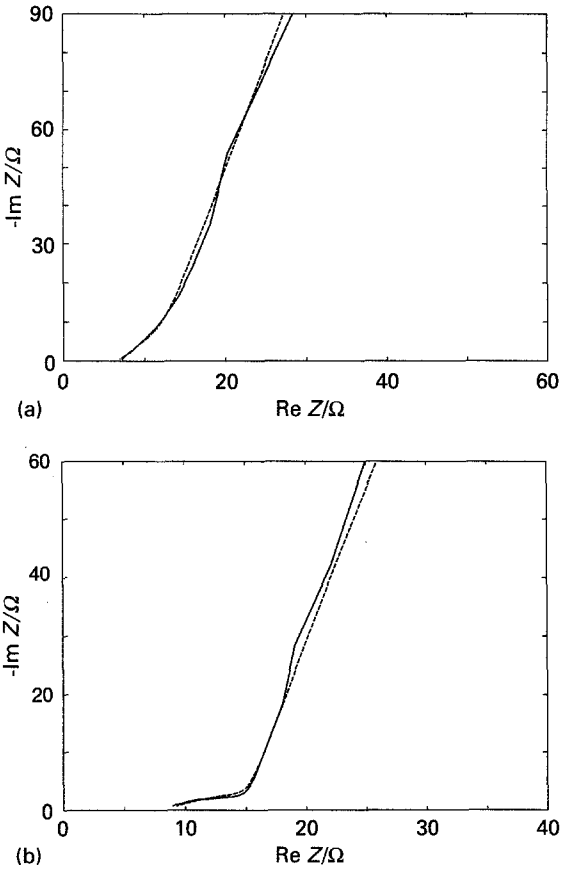

Fig. 8. Nyquist diagrams for the pore shapes of Fig. 7. (a) Pore shape a. (b) Pore shape b. Key: (——) measured; (- - - -) method 2.

pores were again made by drilling. The two shapes used are shown in Fig. 7. Shape a has a narrowing cross section seen from the pore mouth, while shape b has a broadening cross section.

Values for the unknown parameter set were again obtained from the measured impedances by the two analysing methods. The value for Λ_g used in method 1 is calculated using the matrix method (Table 2). In method 2 the matrix method is used, since no analytical solution is available. It was shown in Part I that the pore with variable section only has to be split in a small number of discs, when this method is used. Both for shape a and b, the part with linearly varying pore radius was divided in five discs ($N = 5$). Increasing N resulted in a negligible change of the calculated impedances. A substantial reduction of N is obtained, compared to the recursion method of Keiser *et al.* With the fitted parameter set, a comparison was made between the measured and simulated impedance data for both shapes, Fig. 8(a) and (b). Since again almost no difference between the simulated impedances from both methods was observed, only values obtained by method 2 are shown in Fig. 8. For both pore shapes a reasonably good agreement is found between the measured and calculated Nyquist curves.

In Table 2 the obtained specific electrolyte resistance values are shown. For pore shape a, the specific electrolyte resistance ρ_s is smaller than the mean value found for cylindrical pores, 3.65 Ωcm, whereas for

pore shape b the contrary is true. The higher ρ_s-value for shape b can be due to the higher r/l-ratio of the cylindrical part of pore b ($r/l = 4/7 = 0.57$). Moreover, it is possible that the current, after passing through the smaller pore mouth, does not spread homogeneously over the cylindrical pore part. It was explained above that this increases the experimentally obtained ρ_s-value.

For method 1, the evaluation can also be expressed in another way. Using Equation 11 of method 1 and assuming that $\rho_s = 3.65\,\Omega\,\text{cm}$, experimental Λ_g-values can be found, namely $\Lambda_g = 0.105$ for shape a and $\Lambda_g = 0.755$ for shape b. This gives experimental evidence that $\Lambda_g < 1/3$ for the pore with narrowing section (a) and $\Lambda_g > 1/3$ for the pore with broadening section (b) as was stated in Part I.

5. Summary and conclusions

Experimental illustration and verification has been given for the theory and the matrix model for the calculation of the impedance of noncylindrical pores presented in Part I. Impedance measurements were performed on pores drilled in AISI 316 and immersed in 0.5 M sulphuric acid.

It was found, from measurements on cylindrical pores, that one-dimensional modelling was possible when the ratio of the pore radius to the pore length is less than 0.5. Since this is mostly the case in practice, many porous electrodes can be modelled with a one-dimensional approach. For higher ratios it was found, from a virtual increase of the fitted specific electrolyte resistivity value, that the current does not spread homogeneously over the pore section. This results in a virtual pore radius which is smaller than the real one.

Measurements of noncylindrical scaled-up pores illustrated the advantages of the matrix model compared to the recursion model of Keiser *et al* [7]. It was found that there was a substantial reduction of the number of discs N into which the pore needs to be split. This provides an advantage in the fitting processes. Moreover, experimental evidence was found for the introduction of a geometry constant Λ_g. A narrowing pore section seen from the pore mouth gave $\Lambda_g < 1/3$, whereas a broadening section gave $\Lambda_g > 1/3$. This confirms the theory of Part I.

References

[1] T. Kenjo, S. Osawa and K. Fujikawa, *J. Electrochem. Soc.* **138** (1991) 349.
[2] S. J. Lenhart, D. D. Macdonald and B. G. Pound, *ibid.* **135** (1988) 1063.
[3] C. Cachet, B. Saidani and R. Wiart, *ibid.* **139** (1992) 644.
[4] J. G. Thevenin and R. H. Muller, *ibid.* **134** (1987) 2650.
[5] D. D. Macdonald, M. Urquidi-Macdonald, S. D. Bhakta and B. G. Pound, *ibid.* **138** (1991) 1359.
[6] K. Eloot, F. Debuyck, M. Moors and A. P. Van Peteghem, *J. Appl. Electrochem.* **25** (1995).
[7] H. Keiser, K. D. Beccu and M. A. Gutjahr, *Electrochim. Acta* **21** (1976) 539.
[8] J. D'Ans and E. Lax, 'Taschenbuch Chemiker und Physiker', Springer-Verlag, Berlin (1949) p. 1225.